Influence of Subsurface Defects on the Surface Reactivity of TiO_2: Water on Anatase (101)

Ulrich Aschauer,*,† Yunbin He,‡,§ Hongzhi Cheng,† Shao-Chun Li,‡ Ulrike Diebold,‡ and Annabella Selloni†

Department of Chemistry, Princeton University, Frick Laboratory, Princeton, New Jersey 08544, Department of Physics, Tulane University, Percival Stern Hall, New Orleans, Louisiana 70118, and Faculty of Material Science and Engineering, Hubei University, Wuchang District Xueyuan Road #11, 430062 Wuhan, Hubei, China

Received: October 27, 2009; Revised Manuscript Received: December 9, 2009

The adsorption of water on a reduced TiO_2 anatase (101) surface is investigated with scanning tunneling microscopy and density functional theory calculations. The presence of subsurface defects, which are prevalent on reduced anatase (101), leads to a higher desorption temperature of adsorbed water, indicating an enhanced binding due to the defects. Theoretical calculations of water adsorption on anatase (101) surfaces containing subsurface oxygen vacancies or titanium interstitials show a strong selectivity for water binding to sites in the vicinity of the subsurface defects. Moreover, the water adsorption energy at these sites is considerably higher than that on the stoichiometric surface, thus giving an explanation for the experimental observations. The calculations also predict facile water dissociation at these sites, confirming the important role of defects in the surface chemistry of TiO_2.

1. Introduction

Titanium dioxide (TiO_2) is a technologically important material used for many applications, most notably, in photocatalysis, including hydrogen production[1] and solar energy conversion.[2] Because most applications take place in an aqueous environment, the reactivity of TiO_2 surfaces with water is of great importance for understanding the nature of the photocatalytic processes occurring on these surfaces. Consequently, many experimental[3–5] and theoretical[6–8] studies have investigated water adsorption on TiO_2 surfaces, focusing, for the most part, on the TiO_2(110) surface of the stable rutile polymorph, where water dissociation in the presence of surface vacancies[9–11] has been clearly established. The anatase phase has received less attention, although, in recent years, interest has increased due to both its predominance in nanosized crystals[12] and its higher photocatalytic activity.[2] The most abundant anatase surface is the (101) face,[13] which is characterized by a sawtooth-like structure with ridges of two-fold coordinated O_{2c} atoms along the [010] direction (Figure 1). It was shown theoretically, and later confirmed by experiment, that water adsorbs molecularly on anatase (101), with the water oxygen (O_w) binding to the five-fold coordinated Ti_{5c} sites, while the water hydrogen atoms (H_w) form H bonds with the O_{2c} atoms on the next ridge (the one to the right of the Ti_{5c} site in Figure 1).[14–17] It was also theoretically predicted that surface vacancies on anatase (101) would lead to water dissociation, as in the case of rutile TiO_2(110).[18] However, anatase was experimentally shown to have a rather low surface vacancy concentration,[19] and more recently, the predominance of intrinsic subsurface defects in anatase has been established.[20,21] The role this dominating type of defects plays in the reactivity of anatase surfaces with water is, so far, unknown; its study is, therefore, important for advancing the current understanding of photocatalytic processes on anatase.

Here, we report results of both scanning tunneling microscopy (STM) experiments and theoretical density functional theory calculations, which elucidate the role of subsurface defects, namely, oxygen vacancies as well as titanium interstitials, in the adsorption and dissociation of water on the anatase (101) surfaces.

2. Materials and Methods

2.1. Experimental Details. All experiments were performed in an ultra-high-vacuum (UHV) chamber with a base pressure of $\sim 1 \times 10^{-10}$ mbar (SPECS GmbH). It is equipped with a variable-temperature Aarhus STM, low-energy electron diffraction (LEED), X-ray photoelectron spectroscopy (XPS), a quadrupole mass spectrometer, ion gun, and gas dosing system. In-situ sample cleaning was achieved by cycles of Ar^+ ion sputtering and annealing to 600 °C.

We conducted our experiments on three different anatase surfaces with varying degrees of nonstoichiometry in the bulk. As we do have not the experimental means to quantitatively characterize the degree of oxygen deficiency in our samples, we refer to them qualitatively as "pristine", "slightly reduced", and "heavily reduced". The first sample was a freshly cleaved mineral, as described in ref 22, and showed no Ti^{3+} states in XPS. The second sample was also a natural mineral crystal, originally orange-clear in color, which became blue and darker with repeated sputtering/annealing cycles. For the "slightly reduced" surface, the sample was subjected to approximately 100 cycles. For the "heavily reduced" surface, the same sample was subjected to another ~80 cycles over the course of 8 months. This surface is described in ref 21; in XPS, the Ti 2p level exhibits ~20% Ti^{3+} states.

Prior to dosing experiments, water was cleaned by repeated freeze−pump−thaw cycles and the purity of water vapor was checked by mass spectrometry. Water was dosed by backfilling the chamber via a leak valve with the sample in the cold stage

* To whom correspondence should be addressed. Phone: 609-258-0116. Fax: 609-258-6746. E-mail: aschauer@princeton.edu.
† Princeton University.
‡ Tulane University.
§ Hubei University.

10.1021/jp910492b
Published on Web 12/22/2009

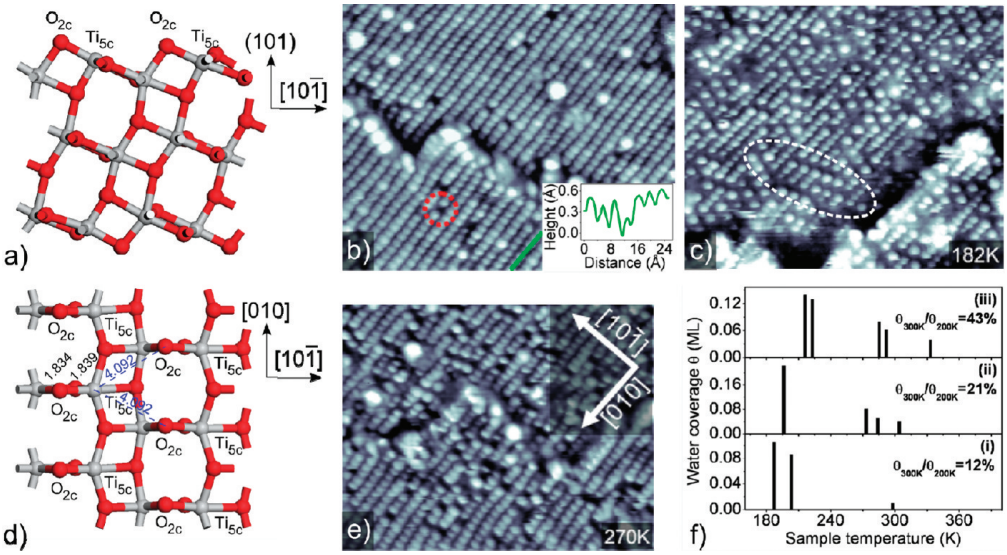

Figure 1. (a) View of the anatase (101) surface along the [010] direction (front view) and (d) top view, showing the two-fold coordinated oxygen (O_{2c}) and the five-fold coordinated (Ti_{5c}) titanium atoms. (b, c, e) STM images (18 nm × 14 nm) of reduced anatase (101). Clean surface (b), the unevenness in the line profile is due to changes in the local electronic structure caused by subsurface defects, and after water dose at T ∼150 K and imaged at 182 K (c) and at 270 K (e). The panel in (f) shows the water coverage θ as a function of sample temperature for samples in three different reduction states: (i) pristine, (ii) slightly reduced, and (iii) heavily reduced.

of the STM. The tip was retracted by ∼1 mm from the sample to avoid tip shadowing effects. Typically, water was dosed at a sample temperature between 100 and 170 K with nominal dosages quoted in langmuir (L, where 1 L equals a dose of 1×10^{-6} Torr·s). STM was performed in the constant-current mode, and empty states were typically imaged with positive sample bias voltages in the range of 0.8−2.5 V and tunneling currents between 0.1 and 1.1 nA.

2.2. Computational Methods. Our DFT calculations are carried out using the generalized gradient approximation (GGA) with the Perdew−Burke−Ernzerhof (PBE) exchange and correlation functional,[23] which has proven to be generally very reliable in many studies of anatase.[13,18] The spin-restricted formalism was employed after verifying that spin-polarized and spin-restricted calculations converged to the same solution in several test cases. Additional spin-polarized DFT+U calculations were employed for selected studies; see section 3.2.3. For all calculations, the Quantum ESPRESSO package[24] was used. Electron−core interactions were described by Vanderbilt ultrasoft pseudopotentials,[25] with electrons from the O 2s, O 2p, Ti 3s, Ti 3p, Ti 3d, and Ti 4s shells treated explicitly. Wave functions were expanded in plane waves up to a kinetic energy cutoff of 25 Ry; a cutoff of 200 Ry was used for the augmented density. Reciprocal space sampling was restricted to the Γ-point, which is justified due to the rather large size of the used simulation cells.

The anatase surface was modeled using a repeated slab geometry, with slabs of three TiO_2 layers and a 10 Å thick vacuum separating periodic images along the direction of the surface normal. We considered both a 3 × 1 (10.262 × 11.310 Å) and a 4 × 1 (10.262 × 15.080 Å) surface supercell, corresponding to slabs of 108 and 144 atoms, respectively (in the absence of point defects). Geometry optimizations were carried out using a damped dynamics[26] until forces were below 10^{-3} au (∼0.05 eV/Å) and atomic mean squared displacements became stationary. First-principle molecular dynamics (FPMD) simulations were performed via the Car−Parrinello method[27] using a time step (δt) of 5 au and a fictitious electron mass (e_{mass}) of 500 au. The deuterium mass (2 amu) was used for hydrogen to allow for a larger time step. The ionic temperature was controlled using a Nose thermostat set to either 110 or 220 K. A thermostat was also applied to the electrons, imposing the kinetic energy needed for the electrons to adiabatically follow the ions.[28,29] Energy barriers and pathways for surface reactions were calculated using the nudged elastic band (NEB) method.[30] The atoms in the bottom layer were kept fixed in all calculations.

3. Results and Discussion

3.1. Experiments. An STM image of a clean, reduced surface, taken at room temperature is shown in Figure 1b. The elliptical "atoms" extend across both surface Ti_{5c} and O_{2c} atoms. From the STM line profiles, it is apparent that the surface is electronically inhomogeneous. As reported recently, these inhomogeneities together with XPS results showing Ti^{3+} states in the surface region are attributed to the presence of reducing subsurface defects.[21] Also apparent are several black, atomic-sized spots with the neighboring "atoms" slightly increased in brightness; see, for example, the circled feature in Figure 1b. This is the typical signature of water molecules adsorbed on anatase (101).[17] The water molecules in Figure 1b stem from the residual gas in the UHV chamber. When water is dosed purposely on the cooled sample, the number of black spots increases with exposure (Figure 1c). As has been shown previously,[17] substrate-mediated interactions lead to a weak ordering of the water molecules (Figure 1c). Along the [010] direction, this interaction is slightly repulsive, resulting in a double periodicity along the rows, whereas a slightly attractive interaction across the rows leads to a diagonal alignment of the water molecules, as can be observed in the highlighted area in Figure 1c. When the sample temperature is raised, water desorbs[16] and the density of adsorbed water molecules decreases (Figure 1e). This is quantified in Figure 1f, where the water coverage as a function of temperature is followed with STM for the three different anatase surfaces. At room temperature, hardly any water is left on the pristine surface, while half of

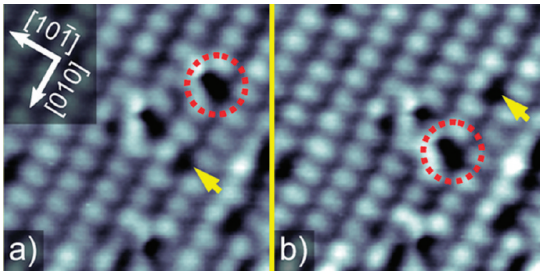

Figure 2. Time lapse STM images showing a water molecule (red circle) migrating on the surface. The final adsorption site marked with a yellow arrow in (a) and the initial adsorption site (yellow arrow in (b)) have the same appearance, indicative of a subsurface defect.

the water that was dosed at lower temperature is still left at the reduced surface.

The time-lapse STM images in Figure 2 show an interesting event during which a water molecule (marked with a red circle) migrates from one subsurface defect site to another (both marked with yellow arrows). The fact that water is not observed in any intermediate state but bound to either defect is strong evidence for preferential water adsorption close to subsurface defect sites. A detailed theoretical analysis of this experimental data will be reported in a forthcoming publication.

3.2. Calculations. ***3.2.1. Water Adsorption in the Presence of Subsurface Oxygen Vacancies.*** *3.2.1.1. Low Water Coverage.* In the 3 × 1 anatase (101) surface supercell used for the calculations, there are six possible Ti_{5c} sites where a water molecule can adsorb. All these sites are equivalent on the stoichiometric surface, but, upon formation of a subsurface vacancy, sites differ, depending on their positions relative to the vacancy. As can be seen from Figure 3a, sites 2 and 3 as well as 4 and 6 are equivalent with respect to the vacancy position, leaving sites 1, 2, 4, and 5 as unique sites. Table 1 gives the molecular water adsorption energies calculated for these sites based on the fully relaxed geometries. It is evident that there is a strong preference for water adsorption on site 5, which is the Ti_{5c} site just to the right of the subsurface vacancy.

The differences in reactivity of the Ti_{5c} sites show a clear correlation with the local structure of these sites (Figure 3a). In particular, a significant lengthening of the $Ti_{5c}-O_{2c}$ bond on the *left* of site 5 is observed (1.881 Å, vs 1.869 Å on the stoichiometric surface); this is accompanied by a shortening of the bond between the same O_{2c} with the Ti_{6c} further to the left (1.791 Å, vs 1.907 Å on the stoichiometric surface). This short $O_{2c}-Ti_{6c}$ bond can be seen as a nearly titanyl-like bond, which is expected to increase the surface reactivity.[31] At all other Ti_{5c} sites, the $Ti_{5c}-O_{2c}$ bond on the left becomes shorter (1.836−1.849 Å). The distances between Ti_{5c} sites and O_{2c} sites on the next ridge toward the *right* (with which a water molecule would form H bonds) show also variations resulting from the presence of the subsurface vacancy. Sites 1 and 5 show a symmetric geometry with $Ti_{5c}-O_{2c}$ distances of 4.08 and 3.98 Å, respectively. For sites 4 and 6, one distance is slightly shorter (4.08 vs 4.05 Å); for sites 2 and 3, one distance is 0.2 Å longer than the other. These structural features are directly reflected in the $Ti_{5c}-O_w$ and H_w-O_{2c} bonding distances of adsorbed water molecules; see Table 1. In particular, a very short $Ti_{5c}-O_w$ bond is present at site 5. Moreover, the water adsorption geometry is asymmetric at site 2, whereas it is perfectly symmetric at sites 1 and 5, with site 5 having very short H_w-O_{2c} bonds (1.985/1.987 Å, vs 2.263/2.257 Å on the stoichiometric surface). These very short bond lengths for site 5 can be also attributed to a significant (∼0.5 Å) outward relaxation of the Ti_{5c} cation at site 5 even before water adsorption.

To further characterize the water adsorption at site 5, we carried out an FPMD simulation of 4.5 ps at 220 K. For most of the duration of the simulation, the water molecule remained bonded with two H_w-O_{2c} hydrogen bonds, as can be seen from the bond-length probability distributions on the right side of Figure 4. It is also evident, however, that, while centered at the equilibrium hydrogen bond length of ∼2 Å, these distributions show a tail toward longer bond lengths. Because the largest fluctuations appear to occur out of phase for the two H_w-O_{2c} bonds, we infer that, at finite temperature, the water molecule can adopt configurations with only one hydrogen bond by a flip motion around the remaining hydrogen bond.

Dissociated configurations for adsorbed water were also studied. These were obtained by moving a hydrogen of an adsorbed water molecule to a neighboring O_{2c} site. Each Ti_{5c} has three nearest O_{2c} neighbors—one to the left and two to the right, top-right and bottom-right—which will be denoted as A, B, and C (inset in Figure 6d), respectively, in the following. The resulting adsorption energies are given in Table 2, where they are compared to the energies of dissociative adsorption on the stoichiometric surface. It can be seen that, in all cases, the energy for dissociative adsorption is less favorable than that for molecular adsorption. The water dissociation barrier at site 5 was quantitatively determined by means of NEB calculations, with the proton moved to neighbor C (Table 3). Although an energy barrier of 0.52 (0.12) eV was computed for the dissociation (recombination) reaction in the absence of subsurface vacancy, this energy is reduced to 0.26 (0.13) eV when the vacancy is present. Such a low value of the dissociation barrier suggests that water dissociation is likely to occur on the reduced surface even at low temperatures (220 K), effectively leading to an equilibrium between molecular and dissociated water molecules on this surface.

The above analyses highlight the important role of surface structure, notably defect-induced surface relaxations, in explaining the different site reactivities, particularly the high reactivity of site 5 toward water adsorption. Defect-induced electronic effects can also influence the surface reactivity. At the GGA level, however, the defect charge distribution is quite delocalized (see Figure 5) and its correlation with the different site reactivities is not straightforward.

3.2.1.2. Effect of Increased Water Coverage. At higher water coverage, a competition between neighboring water molecules for bonding to O_{2c} sites is present.[17] As a result, half monolayer configurations with alternating free and occupied Ti_{5c} sites along the [010] direction are energetically more favorable than a full monolayer where each Ti_{5c} site is occupied by a water molecule. The study of the half monolayer configuration requires an even number of Ti_{5c} sites along [010]; thus, a reduced 4 × 1 (101) anatase supercell was used in this study.

The average molecular adsorption energy per water molecule in the half monolayer is −0.713 eV on the stoichiometric surface and −0.774 eV on the reduced surface; the corresponding configurations with one dissociated water molecule have average adsorption energies of −0.369 and −0.671 eV, respectively. Thus, water dissociation is still an uphill reaction; however, compared with isolated water molecules, the energy difference decreases by 0.213 eV on the reduced and 0.039 eV on the stoichiometric surface due to the presence of the other molecules in the half monolayer. The computed energy barrier (Table 3) for dissociation (recombination) at the most favorable adsorption site is 0.26 (0.16) eV, to be compared to 0.53 (0.18) eV on the

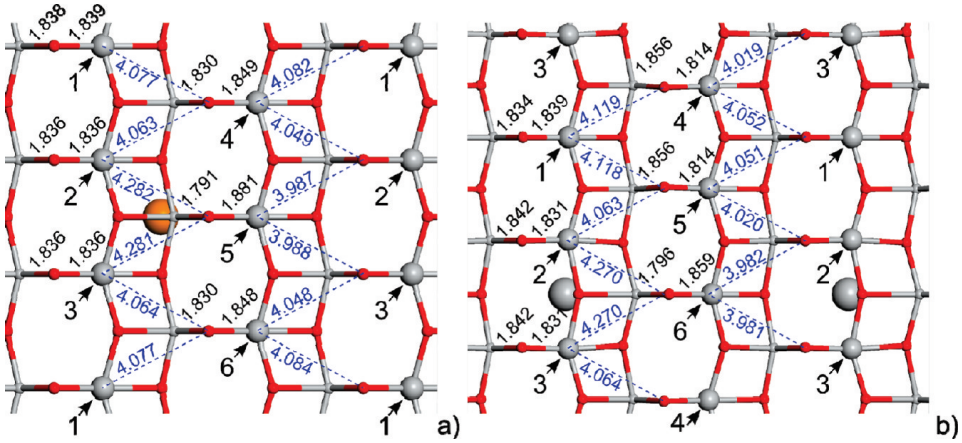

Figure 3. Ti_{5c} sites (1−6, marked with arrows) and interatomic distances on the anatase (101) 3 × 1 surface supercell with (a) an oxygen vacancy (location shown by orange sphere) and with (b) a Ti interstitial (shown as an oversized sphere). Color code: O = red, Ti = gray.

TABLE 1: Adsorption Energy and Bond Distances for a Water Molecule on the Defect-Free (Stoichiometric) Surface and on Defective Surfaces with a Subsurface Oxygen Vacancy or a Titanium Interstitial, Calculated at the GGA-PBE Level[a]

surface	site[b]	ΔE_{GGA} [eV][c]	$Ti_{5c}-O_w$ [Å][c]	H_w-O_{2c} [Å][c]	H_w-O_{2c} [Å][c]
stoichiometric		**−0.7197**	**2.300**	**2.263**	**2.257**
oxygen vacancy	1	−0.7429	2.296	2.198	2.193
	2	−0.6702	2.316	2.061	2.929
	4	−0.7619	2.289	2.250	2.112
	5	**−1.0172**	**2.192**	**1.987**	**1.985**
Ti interstitial	1	−0.6699	2.319	2.185	2.177
	2	**−1.0442**	**2.209**	**2.108**	**2.018**
	4	−0.7913	2.273	2.038	2.187
	6	−0.8599	2.234	2.047	2.040

[a] Calculations were performed using a slab of three TiO_2 layers with a 3 × 1 surface supercell. [b] Surface sites are indicated as in Figure 3. [c] Bold characters are used to indicate the most favorable adsorption site on each different surface.

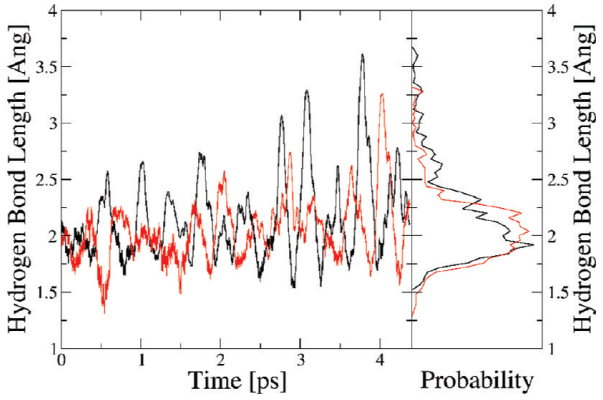

Figure 4. Time evolution of the H_w-O_{2c} hydrogen bond lengths during an FPMD simulation at 220 K of a water molecule adsorbed at site 5 on the anatase (101) surface with a subsurface vacancy. The right side shows the probability distribution of the hydrogen bond lengths, which peaks at the equilibrium value of approximately 2 Å.

stoichiometric surface. A higher surface concentration of water thus favors dissociation on both the stoichiometric and the reduced surface, the effect being much more marked on the latter. In fact, spontaneous water dissociation was observed during FPMD simulations at 220 K on the picosecond time scale.

3.2.2. Water Adsorption in the Presence of Subsurface Ti Interstitials. Ti interstitials are another important type of intrinsic defects; together with oxygen vacancies, they represent the major source of reduction of TiO_2.[32–34] DFT calculations on the binding and diffusion of Ti interstitials at the anatase (101) surface have been reported recently.[35] The influence of these defects on the surface reactivity is expected to be more pronounced than that of oxygen vacancies as a Ti interstitial was recently shown[36] to donate three electrons to the lattice, whereas an oxygen vacancy can donate, at most, two electrons. Here, we study the effect of an interstitial in a subsurface site close to the surface; this site is energetically stable (local minimum), although less stable than sites deeper below the surface.[35]

Using the same procedure employed for the oxygen vacancy, we examined the adsorption of a water molecule at all nonequivalent Ti_{5c} sites in our 3 × 1 surface supercell (see Figure 3b). The results are given in Table 1. Just as seen for the subsurface oxygen vacancy, the Ti interstitial leads to geometry changes on the surface, such as a slight lengthening of the $O_{2c}-Ti_{6c}$ bond lengths to the left of sites 2 and 3 and a significant lengthening and shortening, respectively, of the $Ti_{5c}-O_{2c}$ and $O_{2c}-Ti_{6c}$ bonds left of site 6. These effects are related to an outward relaxation of the Ti_{5c} atoms at sites 2 and 3, which are directly above the interstitial, as well as the Ti_{6c} atom on the right of the interstitial. As a result of these relaxations, the O_{2c} atom left of site 6 also relaxes outward. As for the oxygen vacancy, these surface relaxations are reflected in the water adsorption structure at the different sites given in Table 1. An asymmetric structure resulting from a rotation of the water molecule is found for site 2 and a less asymmetric one for site 4. Sites 1 and 6 are rather symmetric, with shorter bond lengths for site 6. The binding energies in Table 1 follow the same tendency, with the least favorable energy for site 1, where the bond lengths are rather long. An increased stability is observed with a shortening of the bond lengths for sites 4

TABLE 2: Adsorption Energies for a Dissociated Water Molecule on the Defect-Free (Stoichiometric) Surface and on Defective Surfaces with a Subsurface Oxygen Vacancy or a Titanium Interstitial, Calculated at the GGA-PBE Level[a]

stoichiometric		oxygen vacancy			Ti interstitial		
O_{2c}	ΔE_{GGA} [eV]	Ti_{5c} site[b]	O_{2c}[c]	ΔE_{GGA} [eV]	Ti_{5c} site[b]	O_{2c}[c]	ΔE_{GGA} [eV]
A	**−0.3366**	1	A	−0.3483	1	A	−0.2256
B	−0.3208		B	−0.2819		B	−0.2359
C	−0.3203		C	−0.2811		C	−0.2359
		2	A	−0.3069	2	A	−0.7497
			B	−0.1584		B	−0.7758
			C	0.1499		C	**−1.1029**
		4	A	−0.3162	4	A	−0.3290
			B	−0.3251		B	−0.2833
			C	−0.3121		C	−0.3080
		5	A	−0.5053	6	A	−0.3701
			B	**−0.7012**		B	−0.5717
			C	**−0.7010**		C	−0.6003

[a] Calculations were performed using a slab of three TiO_2 layers with a 3 × 1 surface supercell. [b] Surface sites are indicated as in Figure 3. [c] O_{2c} specifies the site of the dissociated proton; see inset in Figure 6d (A = left, B = top-right, C = bottom-right).

TABLE 3: Dissociation (Recombination) Barriers for Water Calculated at the GGA-PBE Level for the Various Surfaces (Stoichiometric and with Subsurface Defects) and as a Function of the Water Coverage (Given in Fractions of a Full Monolayer)

defect	coverage [ML]	barrier [eV]
none (stoichiometric)	1/6	0.52 (0.12)
none (stoichiometric)	1/2	0.53 (0.18)
vacancy (site 5)	1/6	0.26 (0.13)
vacancy (site 5)	1/2	0.26 (0.16)
interstitial (site 2)	1/6	0.24 (0.27)

and 6. The water binding energy is high also at site 2, despite the asymmetric configuration.

The adsorption energies for the dissociated adsorption states are given in Table 2. By comparison with the results in Table 1, we can see that, while on most sites, molecular adsorption is favored, the dissociated state at site 2 (with proton on neighbor C) is the most stable configuration for adsorbed water in the presence of a subsurface Ti interstitial. This favorable dissociation may be, in part, attributed to the presence of the defect-induced localized electronic charge[37] (in the case of a Ti interstitial, partial localization of the excess charge is present also at the GGA level; see Figure 5c). Dissociation at site 2 was observed in FPMD simulations at 110K, suggesting that the energy barrier for dissociation should be small. In fact, the barriers calculated using the NEB method (Table 3) are 0.24 eV for dissociation and 0.27 eV for recombination, which is a significant change from the 0.52 eV/0.12 eV reported above for the stoichiometric surface. Selected configurations along the NEB dissociation pathway are shown in Figure 6.

3.2.3. DFT+U Calculations of Water Adsorption in the Presence of Subsurface O Vacancies. It is known that local and semilocal DFT functionals do not provide a satisfactory description of the character of the electronic defect states in

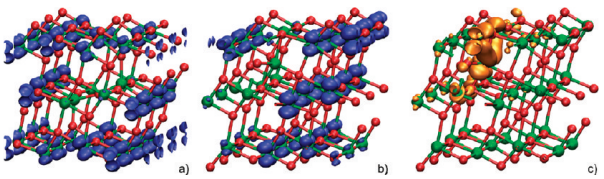

Figure 5. GGA charge density (HOMO = blue and HOMO−1 = orange) of the excess electrons originating from (a) a subsurface oxygen vacancy and (b, c) a Ti interstitial. O = red, Ti=green.

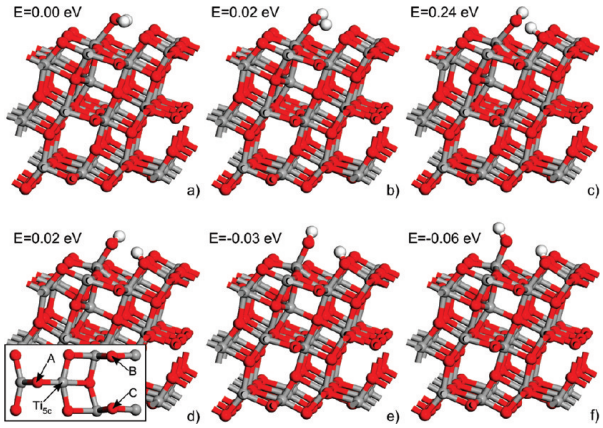

Figure 6. Selected configurations along the dissociation pathway of water at site 2 on the surface with a Ti interstitial: (a) molecularly adsorbed configuration, (b−e) intermediate steps, and (f) dissociated configuration. The transition state is shown in (c). The inset in (d) shows the possible sites (A, B, C) for the proton resulting from the dissociation of the water molecule at the Ti_{5c} site. Color code: O = red, Ti = gray, H = white.

TiO_2.[11,38–40] This is mainly a consequence of the insufficient cancellation of the self-interaction energy,[41] which favors an unphysical delocalization of the electronic states. Similarly, DFT-GGA does not correctly predict the position of the defect energy levels in the band gap. Although the precise character (i.e., amount of localization) of defect states in TiO_2 is not yet well-established,[42] it is interesting to explore how their localization affects the structure and energetics of water adsorption. To this end, we have carried out spin-polarized GGA+U calculations on a slab of three TiO_2 layers with a 3 × 1 surface supercell. We used U = 3.5 eV, which is consistent with previous studies[39,43] and close to the GGA calculated value of U = 3.3 eV[44] for anatase TiO_2. With U = 3.5 eV, the excess electrons originating from the oxygen vacancy form a triplet state on the clean surface with each electron localized on a single Ti atom (site 5) on each of the two slab surfaces; see Figure 7a. (In a previous paper,[35] we showed that one of the localized sites was on a second-layer Ti. The current calculations do not contradict previous results since, here, a smaller slab was used and the two surfaces of the present one are symmetric with respect to the vacancy site.) The two energy levels of the excess electrons are 1.22 and 1.32 eV below the conduction band edge, respectively.

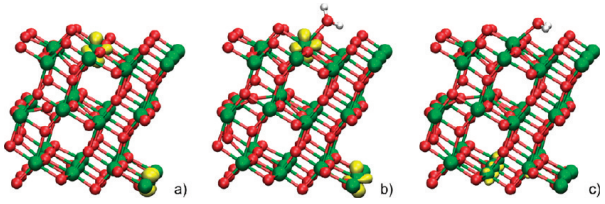

Figure 7. GGA+U spin density (yellow) for (a) the clean slab with a subsurface oxygen vacancy, (b) water adsorbed at site 5 on the same slab, forming one hydrogen bond, and (c) forming two hydrogen bonds, showing the localization of the excess electrons. Color code: Ti = green, O = red, H = white.

TABLE 4: Adsorption Energy and Bond Distances for a Water Molecule on the Defective Surfaces with a Subsurface Oxygen Vacancy, Calculated at the GGA+U Level, with *U* = 3.5 eV

surface	site	ΔE_{GGA+U} [eV]	$Ti_{5c}-O_w$ [Å]	H_w-O_{2c} [Å]	H_w-O_{2c} [Å]
oxygen vacancy	1	−0.7260	2.287	2.247	4.223
	2	−0.6635	2.322	2.288	4.341
	4	−0.8415	2.267	2.044	2.274
	5	**−0.9702**	**2.219**	**1.967**	**4.146**

For molecularly adsorbed water at the four nonequivalent Ti_{5c} sites of the 3 × 1 surface supercell (Figure 3), the GGA+U calculations give the same order of stability as the GGA calculations (see Table 4). Excess electrons remain localized at the same sites as on the clean surface, and their energy levels remain at positions about 1.3 eV below the conduction band edge. At variance with the DFT-GGA calculations, however, GGA+U not always favors the formation of two H bonds of the adsorbed water molecule with surface O_{2c} atoms. In fact, for all adsorption sites except 4, the most stable atomic configuration has only one H bond between the adsorbed water and an adjacent O_{2c}, as is evident from the interatomic distances in Table 4. Stable atomic structures with two H bonds can also be realized but are energetically less favorable. Analysis of the spin densities shows that these less favorable atomic configurations have the excess electrons localized at places different from where they are on the clean surface (Figure 7b,c). This suggests that the formation of two H bonds somehow prevents excess electrons from localizing at their preferred locations, thus making the formation of a single H bond energetically more favorable than forming two H bonds.

Interestingly, the relative stability of the configurations with one and two H bonds appears to be quite sensitive to the value of *U*: we found, indeed, that decreasing *U* from 3.5 to 3.0 eV favors again the formation of two H bonds at site 5, the difference in energy between the two solutions being, in both cases, of the order of 0.1 eV. Most importantly, however, the GGA+U calculations confirm the picture of water adsorption emerging from the GGA calculation, notably the fact that adsorption of water in proximity of a subsurface defect is favored and much stronger than on the stoichiometric surface.

4. Conclusions

In this work, we have presented a combined experimental and first-principles DFT study of water adsorption on reduced anatase (101), a surface where defects mainly occur at subsurface sites.[21] Our STM results show that the presence of subsurface defects, which are prevalent on reduced anatase (101), leads to a higher desorption temperature of adsorbed water, indicating an enhanced binding due to the defects. This interpretation is strongly supported by DFT calculations, which show that certain sites above subsurface vacancies and interstitials are very favorable for water adsorption due to surface relaxation and charge localization effects. While the dissociated state is energetically not favorable in the presence of a vacancy, the barrier for dissociation is small enough to allow for a small population of dissociated water molecules. For subsurface Ti interstitials, the dissociated configuration is even slightly favorable in terms of energy. These results elucidate the role of the prevailing subsurface defects on water adsorption and dissociation on the (101) surface of anatase and, more generally, show the important influence of subsurface defects on the surface chemistry of metal oxides.

Acknowledgment. This work was supported by the DOE-BES (DE-FG02-05ER15702). Princeton Tigress & NERSC facilities are acknowledged for CPU time.

References and Notes

(1) Fujishima, A.; Honda, K. *Nature* **1972**, *238*, 37.
(2) Kavan, L.; Gratzel, M.; Gilbert, S. E.; Klemenz, C.; Scheel, H. J. *J. Am. Chem. Soc.* **1996**, *118*, 6716.
(3) Kurtz, R. L.; Stockbauer, R.; Madey, T. E.; Román, E.; De Segovia, J. L. *Surf. Sci.* **1989**, *218*, 178.
(4) Hugenschmidt, M. B.; Gamble, L.; Campbell, C. T. *Surf. Sci.* **1994**, *302*, 329.
(5) Henderson, M. A. *Surf. Sci.* **1996**, *355*, 151.
(6) Goniakowski, J.; Gillan, M. J. *Surf. Sci.* **1996**, *350*, 145.
(7) Lindan, P. J. D.; Harrison, N. M.; Holender, J. M.; Gillan, M. J. *Chem. Phys. Lett.* **1996**, *261*, 246.
(8) Lindan, P. J. D.; Harrison, N. M.; Gillan, M. J. *Phys. Rev. Lett.* **1998**, *80*, 762.
(9) Brookes, I. M.; Muryn, C. A.; Thornton, G. *Phys. Rev. Lett.* **2001**, *87*, 266103.
(10) Schaub, R.; Thostrup, R.; Lopez, N.; Lægsgaard, E.; Stensgaard, I.; Nørskov, J. K.; Besenbacher, F. *Phys. Rev. Lett.* **2001**, *87*, 266104.
(11) Diebold, U. *Surf. Sci. Rep.* **2003**, *48*, 53.
(12) Zhang, H. Z.; Banfield, J. F. *J. Mater. Chem.* **1998**, *8*, 2073.
(13) Lazzeri, M.; Vittadini, A.; Selloni, A. *Phys. Rev. B* **2001**, *63*, 155409.
(14) Vittadini, A.; Selloni, A.; Rotzinger, F. P.; Grätzel, M. *Phys. Rev. Lett.* **1998**, *81*, 2954.
(15) Tilocca, A.; Selloni, A. *Langmuir* **2004**, *20*, 8379.
(16) Herman, G. S.; Dohnálek, Z.; Ruzycki, N.; Diebold, U. *J. Phys. Chem. B* **2003**, *107*, 2788.
(17) He, Y. B.; Tilocca, A.; Dulub, O.; Selloni, A.; Diebold, U. *Nat. Mater.* **2009**, *8*, 585.
(18) Tilocca, A.; Selloni, A. *J. Chem. Phys.* **2003**, *119*, 7445.
(19) Hebenstreit, W.; Ruzycki, N.; Herman, G. S.; Gao, Y.; Diebold, U. *Phys. Rev. B* **2000**, *62*, R16334.
(20) Cheng, H. Z.; Selloni, A. *Phys. Rev. B* **2009**, *79*, 092101.
(21) He, Y. B.; Dulub, O.; Cheng, H. Z.; Selloni, A.; Diebold, U. *Phys. Rev. Lett.* **2009**, *102*, 106105.
(22) Dulub, O.; Diebold, U. *J. Phys.: Condens. Matter*, in press.
(23) Perdew, J. P.; Burke, K.; Ernzerhof, M. *Phys. Rev. Lett.* **1996**, *77*, 3865.
(24) Giannozzi, P.; Baroni, S.; Bonini, N.; Calandra, M.; Car, R.; Cavazzoni, C.; Ceresoli, D.; Chiarotti, G. L.; Cococcioni, M.; Dabo, I.; Dal Corso, A.; de Gironcoli, S.; Fabris, S.; Fratesi, G.; Gebauer, R.; Gerstmann, U.; Gougoussis, C.; Kokalj, A.; Lazzeri, M.; Martin-Samos, L.; Marzari, N.; Mauri, F.; Mazzarello, R.; Paolini, S.; Pasquarello, A.; Paulatto, L.; Sbraccia, C.; Scandolo, S.; Sclauzero, G.; Seitsonen, A. P.; Smogunov, A.; Umari, P.; Wentzcovitch, R. M. *J. Phys.: Condens. Matter* **2009**, *21*, 395502.
(25) Vanderbilt, D. *Phys. Rev. B* **1990**, *41*, 7892.
(26) Tassone, F.; Mauri, F.; Car, R. *Phys. Rev. B* **1994**, *50*, 10561.
(27) Car, R.; Parrinello, M. *Phys. Rev. Lett.* **1985**, *55*, 2471.
(28) Blöchl, P. E.; Parrinello, M. *Phys. Rev. B* **1992**, *45*, 9413.
(29) Fois, E. S.; Penman, J. I.; Madden, P. A. *J. Chem. Phys.* **1993**, *98*, 6361.
(30) Henkelman, G.; Uberuaga, B. P.; Jónsson, H. *J. Chem. Phys.* **2000**, *113*, 9901.
(31) Di Valentin, C.; Tilocca, A.; Selloni, A.; Beck, T. J.; Klust, A.; Batzill, M.; Losovyj, Y.; Diebold, U. *J. Am. Chem. Soc.* **2005**, *127*, 9895.
(32) Li, M.; Hebenstreit, W.; Diebold, U.; Tyryshkin, A. M.; Bowman, M. K.; Dunham, G. G.; Henderson, M. A. *J. Phys. Chem. B* **2000**, *104*, 4944.

(33) Li, M.; Hebenstreit, W.; Diebold, U.; Henderson, M. A.; Jennison, D. R. *Faraday Discuss.* **1999**, 245.

(34) Wendt, S.; Sprunger, P. T.; Lira, E.; Madsen, G. K. H.; Li, Z. S.; Hansen, J. O.; Matthiesen, J.; Blekinge-Rasmussen, A.; Laegsgaard, E.; Hammer, B.; Besenbacher, F. *Science* **2008**, *320*, 1755.

(35) Cheng, H. Z.; Selloni, A. *J. Chem. Phys.* **2009**, *131*, 054703.

(36) Finazzi, E.; Di Valentin, C.; Pacchioni, G. *J. Phys. Chem. C* **2009**, *113*, 3382.

(37) Tilocca, A.; Selloni, A. *J. Phys. Chem. B* **2004**, *108*, 4743.

(38) Di Valentin, C.; Pacchioni, G.; Selloni, A. *Phys. Rev. Lett.* **2006**, *97*, 166803.

(39) Finazzi, E.; Di Valentin, C.; Pacchioni, G.; Selloni, A. *J. Chem. Phys.* **2008**, *129*, 154113.

(40) Kruger, P.; Bourgeois, S.; Domenichini, B.; Magnan, H.; Chandesris, D.; Le Fevre, P.; Flank, A. M.; Jupille, J.; Floreano, L.; Cossaro, A.; Verdini, A.; Morgante, A. *Phys. Rev. Lett.* **2008**, *100*, 055501.

(41) Cohen, A. J.; Mori-Sanchez, P.; Yang, W. T. *Science* **2008**, *321*, 792.

(42) Di Valentin, C.; Pacchioni, G.; Selloni, A. *J. Phys. Chem. C* **2009**, *113*, 20543.

(43) Morgan, B. J.; Watson, G. W. *Surf. Sci.* **2007**, *601*, 5034.

(44) Mattioli, G.; Filippone, F.; Alippi, P.; Bonapasta, A. A. *Phys. Rev. B* **2008**, *78*, 241201.

JP910492B